AIMS Mathematics, 10(10): 22850–22868.
DOI: 10.3934/math.20251015
Received: 04 August 2025
Revised: 07 September 2025
Accepted: 10 September 2025
Published: 09 October 2025

https://www.aimspress.com/journal/Math

Research article

Asymmetric Lyapunov-Krasovskii functional-driven adaptive event-triggered LFC for semi-Markovian power systems

Kaibo Shi[1,2], Chuan Liu[2,*], Yuping Zhang[1], Xiangkun Wang[2], Yanbin Sun[3] and Xiao Cai[3]

[1] School of Automation Engineering, University of Electronic Science and Technology of China, Chengdu, China
[2] College of Electronic Information and Electrical Engineering, Chengdu University, Chengdu, China
[3] Cyberspace Institute of Advanced Technology, Guangzhou University, Guangzhou, China

* **Correspondence:** Email: 13568594953@163.com.

Abstract: This paper proposes an innovative semi-Markov jump power system H_∞ load frequency control (LFC) strategy, incorporating an adaptive event-triggered mechanism (AETM) to enhance control efficiency and stability under complex environmental conditions. Specifically, to address power system uncertainties caused by environmental factors, we first modeled the system using a semi-Markov jump process, effectively capturing its dynamic variations across different operational states. Subsequently, to reduce communication and computational burdens, we introduced a novel AETM that selectively determines triggering conditions, thereby avoiding unnecessary control signal updates. Furthermore, we constructed multimodal asymmetric Lyapunov-Krasovskii functionals (LKFs). By relaxing constraints on matrix symmetry and positive definiteness, this method reduces the conservatism of stability criteria, ensuring stable system operation and maintaining strong robustness even in the presence of external disturbances. Finally, simulation results validated the effectiveness of the proposed strategy, demonstrating its capability to significantly enhance power system control performance and stability while effectively reducing resource consumption.

Keywords: semi-Markov jump; Lyapunov-Krasovsky functionals; load frequency control; adaptive event-triggered mechanism
Mathematics Subject Classification: 93-XX

1. Introduction

Modern power systems are increasingly challenged by the large-scale integration of renewable energy sources (RESs), dynamic fluctuations in load demand, and growing environmental disturbances. The intermittency and unpredictability of RESs (wind and solar) exacerbate power grid fluctuations,

while environmental factors such as extreme weather and equipment failures amplify operational uncertainties [1–3]. Traditional control methods, predominantly based on linearized models and deterministic assumptions, struggle to address these strong nonlinearities and time-varying characteristics, particularly during stochastic mode transitions triggered by environmental factors [4]. Consequently, developing novel strategies capable of accurately modeling environmental uncertainties and achieving efficient robust control has become critical for ensuring the secure and stable operation of power systems under complex conditions [5, 6].

LFC is a cornerstone for maintaining frequency stability and balancing generation-demand in interconnected grids [7]. Conventional LFC methods perform adequately under steady-state conditions but exhibit significant limitations in handling time-varying communication delays, parameter perturbations, and abrupt mode switching induced by environmental disturbances [8–10]. Recent advancements have incorporated robust control theories, such as H_∞ control, to enhance disturbance rejection capabilities [11, 12]. However, existing studies often rely on fixed-topology assumptions or idealized Markov jump processes (MJPs) [13], neglecting the semi-Markov jump system (S-MJS) nature of real-world power systems, where mode dwell times follow non-exponential distributions and are closely tied to environmental factors [14–16]. This oversight limits the adaptability of current strategies in complex environments, necessitating S-MJS modeling to accurately characterize system dynamics driven by environmental uncertainties.

To alleviate the communication and computational burden in networked control systems, the event-triggered mechanism (ETM) has been proposed as a promising paradigm [17, 18]. Unlike traditional time-triggered approaches, the ETM updates control signals only when predefined triggering conditions are violated, thereby significantly reducing redundant data transmission [19]. Literature [20] first investigated a discrete system state-based ETM, demonstrating its effectiveness in controlling data transmission volume and alleviating bandwidth pressure. Subsequently, Cheng et al. [21] proposed a distributionally robust optimization-based stochastic model predictive control algorithm incorporating the ETM. Following a similar approach, researchers developed a stochastic sampling control method adhering to the Bernoulli distribution to reduce channel occupancy [22]. Furthermore, Yang et al. [23] introduced a dynamic memory ETM, whose core innovation lies in setting the threshold (or data volume) associated with triggering conditions as a dynamically adjustable variable responsive to error functions. However, in scenarios where environmental disturbances cause random state switching in power systems, existing fixed-threshold ETMs exhibit critical limitations. Their rigid triggering parameters struggle to effectively respond to dynamic error coupling induced by state transitions; concurrently, thresholds set to maintain system stability during frequent state switching tend to trigger communication resource overload [24, 25]. To address these limitations of static triggering logic in random state-switching environments, this study aims to develop an AETM, designed to holistically balance system stability and control efficiency.

In stability analysis of time-delay and switching systems, LKFs serve as fundamental tools. Traditional LKFs impose strict symmetry and positive definiteness on weighting matrices, resulting in overly conservative stability criteria [26]. To address this, relaxed LKFs were developed by decoupling matrix symmetry constraints. For instance, [27] utilized augmented matrix techniques to relax symmetry requirements, and [28] refined delay-dependent criteria via integral inequalities. A breakthrough came with asymmetric LKFs, which permit non-symmetric and semi-positive-definite matrices, significantly enhancing analytical flexibility [29]. [30] demonstrated the superior robustness

of asymmetric LKFs in networked control systems with time-varying delays. Nevertheless, existing asymmetric LKF studies focus on single-mode or MJP systems, failing to address multimodal S-MJS or integrate with LFC engineering practices. This theoretical limitation hinders their ability to tackle the intertwined challenges of environmental disturbances and multimodal switching in power systems.

Building upon the preceding discussion, this paper primarily addresses the LFC challenge and introduces a stochastic stability condition for power systems guaranteeing H_∞ performance. The paper's contributions are threefold:

(1) A semi-Markov jump-based power system model is proposed, which effectively captures uncertain dynamic variations under complex environmental conditions and establishes a control framework adaptable to various operational states.

(2) We introduce a novel AETM that dynamically adjusts triggering conditions, significantly reducing communication costs and computational burden by avoiding unnecessary control signal updates while maintaining control performance.

(3) Breaking through the strict restriction that traditional LKFs require symmetric positive-definite matrices, mode-dependent asymmetric LKFs have been constructed, and more relaxed stability criteria have been derived.

Notation: He$\{W\}$ refers to $W+W^T$. Superscripts T and -1 indicate the transpose and inverse forms, respectively. The notation $Q<0$ is used to denote that Q is a negative definite matrix.

2. Preliminaries

The present discussion first employs a semi-Markov jump model to capture state transitions in the power system, establishing a power system model incorporating electric vehicles (EVs). Then it proposes an AETM to enhance triggering effectiveness by dynamically adjusting triggering parameters.

2.1. System descript

Figure 1 illustrates a power system model equipped with an AETM. By integrating this model with a semi-Markov model, the following differential equation is constructed:

$$\begin{cases} \Delta\dot{P}_V(t) = \frac{1}{T_g^{l_t}}\left(\beta_g^{l_t}u(t) - \frac{1}{R^{l_t}}\Delta f(t) - \Delta P_V(t)\right), \\ \Delta\dot{P}_G(t) = \frac{1}{T_t^{l_t}}\left(\Delta P_V(t) - \Delta P_G(t)\right), \\ \Delta\dot{f}(t) = \frac{1}{T_p^{l_t}}\left(\Delta P_G(t) + \Delta P_e(t) - w(t) - L_p^{l_t}\Delta f(t)\right), \\ \Delta\dot{P}_e(t) = \frac{1}{T_e^{l_t}}\left(\beta_e^{l_t}K_e^{l_t}u(t) - \varphi_e^{l_t}K_e^{l_t}\Delta f(t) - \Delta P_e(t)\right), \end{cases}$$

where the parameters with corresponding explanations have been carried out in the Table 1.

Table 1. Figure 1 parameter description.

Symbols	Practical significance	Symbols	Practical significance
ΔP_V	Valve position error	ACE	Regional deviation
ΔP_G	Generation tracking error	R	Governor droop characteristic
$\Delta f(t)$	Frequency deviation	φ_e	EVs droop characteristic
ΔP_d	Load disturbance	K_e	EVs gain
ΔP_e	Incremental changes in EVs	δ	Frequency bias constant

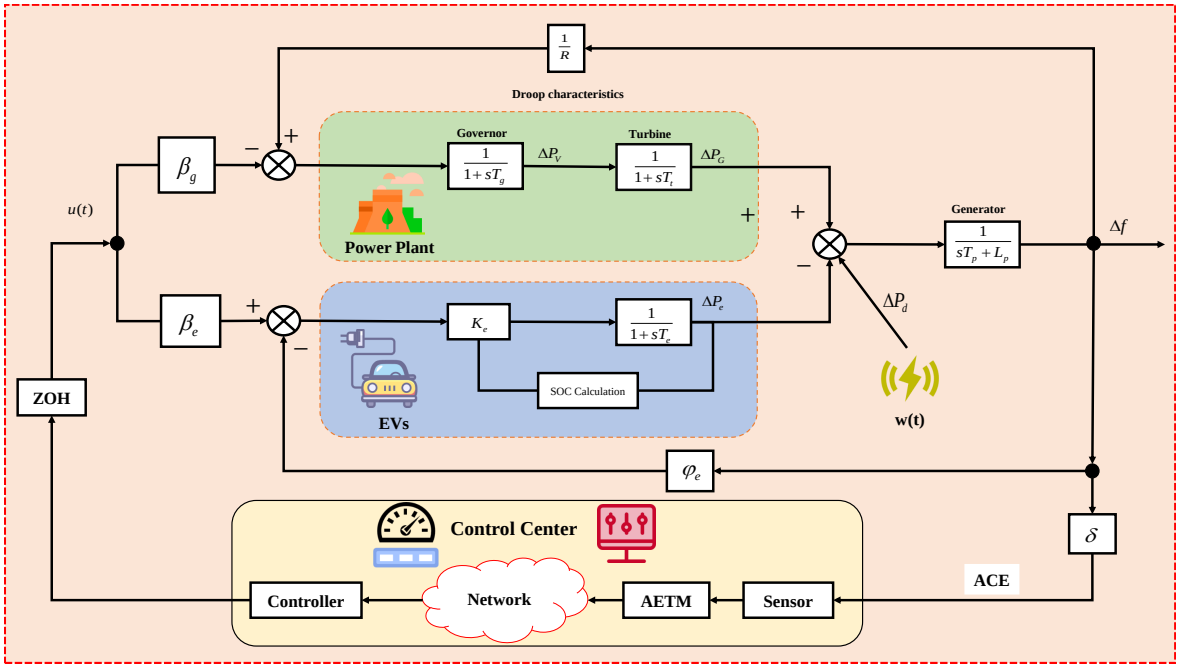

Figure 1. Schematic of the AETM-equipped power system.

The state vector is constructed as $x(t) = \text{col}\{\Delta P_V(t), \Delta P_G(t), \Delta f(t), \Delta P_e(t), \int ACE(t)\}$. The system's control output is given by $u(t) = -Ky(t)$, with $w(t) = \Delta P_d(t)$ denoting the disturbance input, and the output vector defined as $y(t) = \text{col}\left\{ACE(t), \int ACE(t)\right\}$. Here, $ACE(t) = \delta^{l_t}\Delta f(t)$ characterizes the area control error.

Accordingly, the system is mathematically represented as:

$$\begin{cases} \dot{x}(t) = A_{l_t}x(t) + B_{l_t}u(t) + F_{l_t}w(t), \\ y(t) = C_{l_t}x(t). \end{cases} \tag{2.1}$$

From this we can derive the system constant matrix as follows:

$$A = \begin{bmatrix} -\frac{1}{T_g^{l_t}} & 0 & -\frac{1}{R^{l_t}T_g^{l_t}} & 0 & 0 \\ \frac{1}{T_t^{l_t}} & -\frac{1}{T_t^{l_t}} & 0 & 0 & 0 \\ 0 & \frac{1}{T_p^{l_t}} & -\frac{L_p^{l_t}}{T_p^{l_t}} & \frac{1}{T_p^{l_t}} & 0 \\ 0 & 0 & -\frac{\varphi_e^{l_t}K_e^{l_t}}{T_e^{l_t}} & -\frac{1}{T_e^{l_t}} & 0 \\ 0 & 0 & \delta & 0 & 0 \end{bmatrix}, \quad B = \begin{bmatrix} \frac{\beta_g}{T_g^{l_t}} \\ 0 \\ 0 \\ \frac{K_e^{l_t}\beta_e^{l_t}}{T_e^{l_t}} \\ 0 \end{bmatrix}, \quad C^T = \begin{bmatrix} 0 & 0 \\ 0 & 0 \\ \delta & 0 \\ 0 & 0 \\ 0 & 1 \end{bmatrix}, \quad F = \begin{bmatrix} 0 & 0 & 0 & 0 & 0 \\ 0 & 0 & 0 & 0 & 0 \\ -\frac{1}{T_P^{l_t}} & 0 & 0 & 0 & 0 \\ 0 & 0 & 0 & 0 & 0 \\ 0 & 0 & 0 & 0 & 0 \end{bmatrix}.$$

Furthermore, $\{l_t, t \geq 0\}$ models a semi-Markov process characterized by switching matrix $\pi = [\pi_{mn}]_{3\times3}$, while its state collection $M = 1, 2, 3$ defines the operational modes. The switching mechanism adheres to:

$$\Pr\{l_{t+\delta} = n \mid l_t = m\} = \begin{cases} \pi_{mn}(h)\delta + o(\delta), & n \neq m, \\ 1 + \pi_{mm}(h)\delta + o(\delta), & n = m, \end{cases} \tag{2.2}$$

with δ being an infinitesimal positive parameter satisfying $\lim_{\delta\to0} o(\delta)/\delta = 0$, off-diagonal elements $\pi_{mn}(h) \geqslant 0$ $(n \neq m)$, and diagonal terms complying with $\pi_{mm}(h) = -\sum_{n\neq m}\pi_{mn}(h)$, holding universally for all $m \in M$.

Remark 2.1. *In practical power system engineering, various unforeseen changes are often encountered, such as sudden weather variations, abrupt environmental shifts, and unexpected equipment failures. These abrupt changes can lead to variations in system parameters. Unlike conventional Markov jumps, we employ semi-Markov jumps that better align with real-world scenarios to describe system transitions. By considering both the time dependency and historical state dependency of system modes, a power system model with semi-Markov jumps is established.*

2.2. Design of the AETM

Assume that the fixed sampling time of the sensor is h, and lh ($l = 1, 2, \ldots$) designates distinct sampling instants of the sensor; $x(lh)$ indicates the state at this sampling time. $t_m h \in \{lh, m \in \mathbb{R}\}$ is the trigger moment, and $t_{m+n}h$ represents the $n_t h$ trigger moment; $x(t_m h)$ indicates the state of the trigger moment. The conventional ETM is constructed according to:

$$t_{m+1}h = t_m h + \min_{l\in\mathbb{N}} \{lh \mid g(x(t_m h), e(l_m h)) > 0\}. \tag{2.3}$$

The triggering criterion function is specified as $g(x(t_m h), e(l_m h)) = e^T(l_m h)\Omega e(l_m h) - \phi x^T(t_m h)\Omega x(t_m h)$. Here $\Omega > 0$ denotes a weighting matrix requiring determination, while $\phi > 0$ constitutes a triggering coefficient. The error term $e(l_k h)$ is prescribed by $e(l_k h) = x(t_m h) - x(l_m h)$, where $x(l_m h) = x(t_m h + lh)$.

The static trigger coefficient in this conventional ETM constitutes a fixed constant, failing to adequately capture the significance of triggering-time data. To enhance closed-loop performance, an AETM is developed using this methodology:

$$t_{m+1}h = t_m h + \min_{l\in\mathbb{N}} \{lh \mid \bar{g}(x(t_m h), e(l_k h)) > 0\}, \tag{2.4}$$

where $\bar{g}(x(t_m h), e(l_m h)) = e^T(l_m h) C^T \Omega C e(l_m h) - \phi(t) x^T(t_m h) C^T \Omega C x(t_m h)$, with the trigger parameter $\phi(t) = \phi_1 + \phi_2 e^{-\phi_3 \left(e^T(l_m h) e(l_m h)\right)^{1/2}}$, and ϕ_1, ϕ_2, ϕ_3 are known constants.

Define $\tau_t = t - t_m h - nh$ ($n = 1, 2, \ldots$). Over the holding window of the zero-order hold (ZOH) $t \in [t_k h = +\tau_t, t_{m+1}h + \tau_{t+1})$, it can be divided into $[t_m h + \tau_t, t_{m+1}h + \tau_{t+1}) = \bigcup_{s=0}^{d_n} Y(n, m)$ with $Y(n, m) = [t_m h + nh + \tau_{t+n}, t_m h + nh + \tau_{t+n+1})$, $n = 1, 2, \ldots, d_n$, $d_n = t_{m+1} - t_m - 1$. Set $\tau(t) = t - t_m h - nh$, $0 \le t_m \le \tau(t) \le h + \tau_{m+n+1} = \tau_M$, and then equation $e(t) = x(t_m h) - x(t_{m+1}h + nh)$ can be transformed into:

$$x(t_m h) = x(t - \tau(t)) + e(t), \quad t \in [t_m h + \tau_k, t_{m+1}h + \tau_{m+1}). \tag{2.5}$$

From the above, we get the semi-Markov jump power system:

$$\begin{cases} \dot{x}(t) = A_m x(t) - B_m K_m C_m (x(t - \tau(t)) + e(t)) + F_m w(t), \\ y(t) = C_m x(t). \end{cases} \tag{2.6}$$

Remark 2.2. *In contrast to the conventional ETM [31], the AETM developed herein employs dynamic triggering parameters that account for state estimation deviations. Specifically, the triggering coefficient is formulated as:* $\phi(t) = \phi_1 + \phi_2 \exp(-\phi_3 |e(l_m h)|_2)$, *where* $|e(l_m h)|_2 = \left(e^T(l_m h) e(l_m h)\right)^{1/2}$. *This formulation effectively resolves triggering failures at critical sampling points that violate the triggering criterion:* $g(x(t_m h), e(l_m h)) = e^T(l_m h)\Omega e(l_m h) - \phi x^T(t_m h)\Omega x(t_m h)$. *Moreover,*

the enhanced triggering condition (2.4) enables adaptive reduction of the triggering frequency, improves controller-actuator data transmission efficiency, mitigates Zeno behavior, and conserves communication bandwidth.

3. Basic lemmas and definitions

Lemma 3.1. *For any positive constant matrix R, and the continuously differentiable function* $x(t) : [\iota_1, \iota_2] \to \mathbb{R}^n$*, the following inequality holds:*

$$-(\iota_2 - \iota_1)\int_{\iota_1}^{\iota_2} \dot{x}^T(u)R\dot{x}(u)du \leq -\lambda_1^T R\lambda_1 - 3\lambda_2^T R\lambda_2,$$

where $\lambda_1 = x(\iota_2) - x(\iota_1), \lambda_2 = x(\iota_2) + x(\iota_1) - \frac{2}{\iota_2-\iota_1}\int_{\iota_1}^{\iota_2} x(u)du$.

Lemma 3.2. *[32] Given a differentiable mapping* $\dot{x}(\cdot) : [\iota_1, \iota_2] \to \mathbb{R}^n$ *and a symmetric positive-definite matrix* $J > 0$*, this inequality holds:*

$$-\int_{\iota_1}^{\iota_2} \dot{x}^T(u)J\dot{x}(u)du \leq -\frac{1}{\iota_2 - \iota_1}\begin{bmatrix} \lambda_1 \\ \lambda_2 \end{bmatrix}^T \begin{bmatrix} J & 0 \\ 0 & 3J \end{bmatrix}\begin{bmatrix} \lambda_1 \\ \lambda_2 \end{bmatrix},$$

where $\lambda_1 = x(\iota_2) - x(\iota_1), \lambda_2 = x(\iota_2) + x(\iota_1) - \frac{2}{\iota_2-\iota_1}\int_{\iota_1}^{\iota_2} x(u)du$.

Lemma 3.3. *[33] Given matrices* $J \in \mathbb{R}^{n\times n}$, $L \in \mathbb{R}^{n\times n}$ *with* $\begin{bmatrix} J & L^T \\ L & J \end{bmatrix}$*, and a scalar* $\delta \in (0, 1)$*, the subsequent relation holds:*

$$\begin{bmatrix} \frac{1}{\delta}J & 0 \\ 0 & \frac{1}{1-\delta}J \end{bmatrix} \geq \begin{bmatrix} J & L^T \\ L & J \end{bmatrix}.$$

Lemma 3.4. *[34] Consider a full-column-rank matrix* $J \in \mathbb{R}^{n\times m}$ *with singular value decomposition* $J = KJ_0^T L$*, where K and L are orthogonal, and* J_0 *is a diagonal matrix featuring positive real diagonal entries sorted in descending order. For any symmetric* $P \in \mathbb{R}^{n\times n}$*, the equation* $PJ = JQ$ *admits a solution* $Q \in \mathbb{R}^{m\times m}$ *if and only if P decomposes as* $P = K\begin{bmatrix} P_1 & 0 \\ 0 & P_2 \end{bmatrix}K^T$*, with subblocks* $P_1 \in \mathbb{R}^{m\times m}$ *and* $P_2 \in \mathbb{R}^{(n-m)\times(n-m)}$.

Definition 3.1. *[35] Given zero initial conditions, the power system (2.6) with* $w(t) = 0$ *achieves stochastic stabilizability when the subsequent criteria are met:*

$$E\left\{\int_0^\infty \|x(u)\|^2 dt\right\} < +\infty.$$

Definition 3.2. *[36] The* H_∞*-performance-guaranteed stochastic stability of power system (2.6) is resolved by establishing its stochastic stabilizability and requiring that, under null initial states, all non-zero disturbances* $w(t) \in [0, \infty]$ *and prescribed attenuation levels* $\gamma > 0$ *satisfy the condition:*

$$E\left\{\int_0^\infty \|y(t)\|^2 dt\right\} < \gamma^2 E\left\{\int_0^\infty \|w(t)\|^2 dt\right\}.$$

4. Main results

Within this segment, two original propositions are established via LKFs to achieve stochastic stabilization of power systems (2.6) with prescribed disturbance attenuation alongside controller synthesis. Under the simplification premise $l_t = m \in \mathcal{M}$, we define these notations:

$$\bar{P}_m^{(r)} = \sum_{n \in M} \pi_{mn} P_n^{(r)}, \quad (n \in M),$$

$$\theta(t) = col\{x(t), x(t-\tau(t)), x(t-h), \omega_1(t), \omega_2(t), \omega_3(t), e(t_k h), \dot{x}(t), \omega(t)\},$$

$$\omega_1(t) = \int_{t-h}^{t} x(u)du, \quad \omega_2(t) = \frac{1}{\tau(t)} \int_{t-\tau(t)}^{t} x(u)du, \quad \omega_3(t) = \frac{1}{h-\tau(t)} \int_{t-h}^{t-\tau(t)} x(u)du,$$

$$e_j = \left[\begin{array}{ccc} 0_{n\times(j-1)} & I_{n\times 1} & 0_{n\times(9-j)} \end{array} \right], \quad (j = 1, 2, ...9).$$

Theorem 4.1. *Here, we have $h > 0$, γ, a specified controller gain matrix K, and an event-triggering matrix Ω. The power system (2.6) exhibits stochastic stability with H_∞ performance characterized by γ if there exist matrices R_i $(i = 1, 2, 3, 4)$, H, $P_m > 0$, and $W > 0$ of appropriate dimensions such that the following linear matrix inequalities (LMIs) hold for every $m \in M$:*

$$\Gamma_1 = \left[\begin{array}{cc} Q_1 + hZ & * \\ \frac{1}{2}Q_2^T - Z^T & \frac{1}{h}Z \end{array} \right] > 0, \quad \Gamma_2 = \left[\begin{array}{cccc} W & * & * & * \\ 0 & 3W & * & * \\ R_1 & R_2 & W & * \\ R_3 & R_4 & 0 & 3W \end{array} \right] \geq 0, \quad \Gamma_3 = \sum_{i=1}^{8} \gamma_i < 0, \tag{4.1}$$

where

$$\begin{aligned}
\gamma_1 &= 2e_1^T P_m e_8 + e_1^T \bar{P}_m e_1, \\
\gamma_2 &= 2e_1^T Q e_8 - e_1^T Q e_3 + e_3^T Q e_8, \\
\gamma_3 &= h^2 e_8^T Z e_8 - 4e_1^T Z e_1 - 2e_1^T Z e_3 + \frac{12}{h} e_1^T Z e_4 + \frac{6}{h} e_1^T Z e_3 - 4e_3^T Z e_3 + \frac{12}{h} e_3^T Z e_4 - \frac{12}{h} e_4^T Z e_4, \\
\gamma_4 &= h^2 e_8^T W e_8 - 4e_1^T W e_1 - 4e_1^T W e_2 + 12e_1^T W e_5 - 8e_2^T W e_2 - 4e_2^T W e_3 + 12e_2^T W e_5 \\
&\quad + 12e_2^T W e_6 - 4e_3^T W e_3 + 12e_3^T W e_6 - 12e_5^T W e_5 - 12e_6^T W e_6, \\
\gamma_5 &= 2e_2^T R_1 e_1 - 2e_2^T R_1 e_2 - 2e_3^T R_1 e_1 + 2e_3^T R_1 e_2 + 2e_2^T R_2 e_1 - 2e_2^T R_2 e_2 + 2e_3^T R_2 e_1 - 2e_3^T R_2 e_2 - 4e_6^T R_2 e_1 \\
&\quad + 4e_6^T R_2 e_2 + 2e_2^T R_3 e_1 + 2e_2^T R_3 e_2 - 4e_2^T R_3 e_5 - 2e_3^T R_3 e_1 - 2e_3^T R_3 e_2 + 4e_3^T R_3 e_5 + 2e_2^T R_4 e_1 \\
&\quad + 2e_2^T R_4 e_2 - 4e_2^T R_4 e_5 + 2e_3^T R_4 e_1 + 2e_3^T R_4 e_2 - 4e_3^T R_4 e_5 - 4e_6^T R_4 e_1 - 4e_6^T R_4 e_2 + 8e_6^T R_4 e_5, \\
\gamma_6 &= \phi(t)(e_2 - e_7)^T C^T \Omega C (e_2 - e_7) - e_7^T C^T \Omega C e_7, \\
\gamma_7 &= 2e_1 H A_m e_1 - 2e_1 H B_m K_m e_7 - 2e_1 H B_m K_m C_m e_2 + 2e_1 H F_m e_9 - 2e_1 H e_8 + 2e_8 H A_m e_1 \\
&\quad - 2e_8 H B_m K_m e_7 - 2e_8 H B_m K_m C_m e_2 + 2e_8 H F_m e_9 - 2e_8 H e_8, \\
\gamma_8 &= e_1^T C^T C e_1 - \gamma^2 e_9^T e_9.
\end{aligned}$$

Proof. Choose the following mode-dependent asymmetric LKFs:

$$V(t) = \sum_{i=1}^{4} V_i(t), \tag{4.2}$$

where

$$\begin{cases} V_1(t) = x^T(t)P_m x(t), \\ V_2(t) = x^T(t)Q\eta(t), \\ V_3(t) = h\int_{t-h}^{t}\int_{u}^{t} \dot{x}^T(v)Z\dot{x}(v)dvdu, \\ V_4(t) = h\int_{-h}^{0}\int_{t+u}^{t} \dot{x}^T(v)W\dot{x}(v)dvdu. \end{cases}$$

Here, $Q = \begin{bmatrix} Q_1 & Q_2 \end{bmatrix}$, $\eta(t) = \begin{bmatrix} x^T(t) & \int_{t-h}^{t} x^T(u)du \end{bmatrix}^T$. By using Jensen's inequality, the following inequality holds:

$$h\int_{u}^{t} \dot{x}^T(u)Z\dot{x}(u)du \geq (x(t)-x(u))^T Z(x(t)-x(u)), \tag{4.3}$$

$$V_3(t) \geq \int_{t-h}^{t} \begin{bmatrix} x(t) \\ x(u) \end{bmatrix}^T \begin{bmatrix} Z & * \\ -Z^T & Z \end{bmatrix} \begin{bmatrix} x(t) \\ x(u) \end{bmatrix} du. \tag{4.4}$$

So, according to (4.3), it can be further deduced that:

$$V_2(t) + V_3(t) \geq \begin{bmatrix} x^T(t) & \int_{t-h}^{t} x^T(u)du \end{bmatrix} \Gamma_1 \begin{bmatrix} x(t) & \int_{t-h}^{t} x(u)du^T \end{bmatrix}^T > 0, \tag{4.5}$$

and therefore, the $V(t)$ is certified to be positive definite.

To analyze the stochastic behavior of $V(t)$, we compute its weak infinitesimal generator $\mathscr{L}$ as follows:

$$\mathscr{L}V(t) = \sum_{i=1}^{4} \mathscr{L}V_i(t), \tag{4.6}$$

where

$$\begin{cases} \mathscr{L}V_1(t) = 2x^T(t)P_m\dot{x}(t) + x^T(t)\bar{P}_m x(t), \\ \mathscr{L}V_2(t) = 2\dot{x}^T(t)Q_1 x(t) - x^T(t)Q_2 x(t-h) + \dot{x}^T(t)Q_2\int_{t-h}^{t} x(u)du, \\ \mathscr{L}V_3(t) = h^2\dot{x}^T(t)Z\dot{x}(t) - h\int_{t-h}^{t} \dot{x}^T(u)Z\dot{x}(u)du, \\ \mathscr{L}V_4(t) = h^2\dot{x}^T(t)W\dot{x}(t) - h\int_{t-h}^{t} \dot{x}^T(u)W\dot{x}(u)du. \end{cases}$$

With reference to Lemma 3.1, one can deduce:

$$\begin{aligned} & -h\int_{t-h}^{t} \dot{x}^T(u)R\dot{x}(u)du \\ & \leq -\begin{bmatrix} x^T(t) & x^T(t-h) & \int_{t-h}^{t} x^T(u)du \end{bmatrix} \zeta_1 \begin{bmatrix} x^T(t) & x^T(t-h) & \int_{t-h}^{t} x^T(u)du \end{bmatrix}^T, \end{aligned} \tag{4.7}$$

where $\zeta_1 = \begin{bmatrix} 4R & * & * \\ 2R & 4R & * \\ -\frac{6}{h}R & -\frac{6}{h}R & \frac{12}{h^2}R \end{bmatrix}$.

According to Lemmas 3.2 and 3.3, we can derive:

$$\begin{aligned} -h\int_{t-h}^{t} \dot{x}^T(u)W\dot{x}(u)du &= h\left(-\int_{t-h}^{t-\tau(t)} \dot{x}^T(u)W\dot{x}(u)du - \int_{t-\tau(t)}^{t} \dot{x}^T(u)W\dot{x}(u)du\right) \\ &\leq -\frac{h}{h-\tau(t)}\begin{bmatrix} G_3 \\ G_4 \end{bmatrix}^T \begin{bmatrix} W & 0 \\ 0 & 3W \end{bmatrix} \begin{bmatrix} G_3 \\ G_4 \end{bmatrix} - \frac{h}{\tau(t)}\begin{bmatrix} G_5 \\ G_6 \end{bmatrix}^T \begin{bmatrix} W & 0 \\ 0 & 3W \end{bmatrix} \begin{bmatrix} G_5 \\ G_6 \end{bmatrix} \end{aligned}$$

$$\leq -\begin{bmatrix} \bar{G}_1 \\ \bar{G}_2 \end{bmatrix}^T \begin{bmatrix} -\frac{h}{h-\tau(t)}\bar{W} & 0 \\ 0 & \frac{h}{\tau(t)}\bar{W} \end{bmatrix} \begin{bmatrix} \bar{G}_1 \\ \bar{G}_2 \end{bmatrix}$$
$$\leq -\begin{bmatrix} \bar{G}_1 \\ \bar{G}_2 \end{bmatrix}^T \begin{bmatrix} \bar{W} & * \\ R & \bar{W} \end{bmatrix} \begin{bmatrix} \bar{G}_1 \\ \bar{G}_2 \end{bmatrix}, \tag{4.8}$$

where

$$G_1 = x(t) - x(t-h), \qquad G_2 = x(t) + x(t-h) - \tfrac{2}{h}\int_{t-h}^{t} x(u)du,$$
$$G_3 = x(t-\tau(t)) - x(t-h), \qquad G_4 = x(t-\tau(t)) + x(t-h) - \tfrac{2}{h-\tau(t)}\int_{t-h}^{t-\tau(t)} x(u)du,$$
$$G_5 = x(t) - x(t-\tau(t)), \qquad G_6 = x(t) + x(t-\tau(t)) - \tfrac{2}{\tau(t)}\int_{t-h}^{t-\tau(t)} x(u)du,$$
$$\bar{G}_1 = \begin{bmatrix} G_3 & G_4 \end{bmatrix}^T, \bar{G}_2 = \begin{bmatrix} G_5 & G_6 \end{bmatrix}^T, \quad \bar{W} = \begin{bmatrix} W & 0 \\ 0 & 3W \end{bmatrix}, R = \begin{bmatrix} R_1 & R_2 \\ R_3 & R_4 \end{bmatrix}.$$

Referring to the AETM expression in (2.4), the following can be derived:

$$e^T\left(l_{k,n}h\right)C^T\Omega Ce\left(l_{k,n}h\right) \leq x^T\left(t_{k,n}h\right)C^T\Omega Cx\left(t_{k,n}h\right). \tag{4.9}$$

According to the system's state equation, we derive the following formulation:

$$2[x(t)+\dot{x}(t)]^T H\left[A_m x(t) - B_m K_m C_m x\left(t-\tau(t)\right) - B_m K_m e\left(m_k h\right) + F_m w(t) - \dot{x}(t)\right] = 0. \tag{4.10}$$

By integrating equations (4.5) through (4.9) and according to inequality (4.10), we obtain the key inequality:

$$\mathscr{L}V(t) \leq \theta^T(t)\sum_{i=1}^{7}\gamma_i\theta(t) \leq 0. \tag{4.11}$$

Second, we consider the H_∞ performance of the system for given any non-zero disturbance $w(t) \in L_2[0,\infty)$. By combining term (4.10) and (4.11), it follows that:

$$\mathscr{L}V(t) \leq \theta^T(t)\sum_{i=1}^{7}\gamma_i\theta(t) + E\left\{y^T(t)y(t) - \gamma^2 w^T(t)w(t)\right\} \leq 0. \tag{4.12}$$

Then, by taking the integral of both sides of (4.12) from 0 to ∞, and due to the negative definiteness of (4.11), it can be derived that

$$E\left\{\int_0^\infty \|y(t)\|_2\,dt\right\} \leq \gamma^2 E\left\{\int_0^\infty \|\omega(t)\|_2\,dt\right\}. \tag{4.13}$$

Therefore, power system (2.6) achieves stochastic stability while ensuring an H_∞ performance bound of γ. The proof is complete. □

Theorem 4.2. *Here, we have $h > 0$, γ, the power system (2.6) exhibiting stochastic stability with H_∞ performance characterized by γ if there exist matrices R_i ($i = 1,2,3,4$), H, $P_m > 0$, and $W > 0$ of appropriate dimensions such that (4.1) and the following LMIs hold for every $m \in M$:*

$$\Gamma_2 = \sum_{i=1}^{8}\bar{\gamma}_i < 0, \tag{4.14}$$

where

$$
\begin{aligned}
&\bar{\gamma}_i = \gamma_i, \quad i = (1, 2, \cdots, 6),\\
&\bar{\gamma}_7 = 2e_1 HA_m e_1 - 2e_1 B_m Y_m e_7 - 2e_1 B_m Y_m C_m e_2\\
&\qquad + 2e_1 HF_m e_q - 2e_1 He_8 + 2e_8 HA_m e_1 - 2e_8 B_m Y_m e_7\\
&\qquad - 2e_8 B_m Y_m C_m e_2 + 2e_8 HF_m e_9 - 2e_8 He_8,\\
&\bar{\gamma}_8 = e_1^T C^T \Omega C e_1 - \gamma^2 e_9^T e_9.
\end{aligned}
$$

Proof. Notice that $H = U \begin{bmatrix} H & 0 \\ 0 & H \end{bmatrix} U^{\mathrm{T}}$ and $B_m = U B_{m0}^T V$. Lemma 3.4 implies the existence of a matrix X_m satisfying the relation $HB_m = B_m X_m$. Next, let $Y_m = X_m K_m$, which gives us $HB_m K_m = B_m X_m K_m = B_m Y_m$. Substituting $HB_m K_m$ with $B_m Y_m$ in Theorem 4.1 yields Theorem 4.2. Hence, from the above analysis, the controller gain matrix is given by $K_m = \left(B_m^{\mathrm{T}} H B_m\right)^{-1} B_m^{\mathrm{T}} B_m Y$. This completes the proof of Theorem 4.2. □

5. Simulation example

5.1. System performance comparis

In this subsection, we compare the stability performance of power system (2.6) under different H_∞ performance indices γ and different transition probabilities π.

Table 2 enumerates the configuration parameters for system (2.6), where the initial state vector is given by $x(0) = \mathrm{col}\{8.5,\ 0,\ -5.5,\ -9.8,\ 7.21\}$. With the sensor sampling interval set to $h = 0.02$, the remaining parameters are defined below: $\tau_M = 0.02, \varphi = 1, w(t) = 0.01, \phi_1 = 0.32, \phi_2 = 0.55, \phi_3 = 0.03, w(t) = 0.01$. Furthermore, under varying performance indices γ and transition probabilities π, the triggering threshold matrix Ω and feedback gain matrix k obtained by solving the linear matrix inequalities (4.14) in Theorem 4.2 are provided in Table 3.

Table 2. Specific values of the parameters.

Mode	Power plant parameters							EV parameters		
	$T_t^{l_t}$	$T_g^{l_t}$	$T_p^{l_t}$	$L_p^{l_t}$	$\beta_e^{l_t}$	R^{l_t}	$\varphi_e^{l_t}$	$T_e^{l_t}$	$K_e^{l_t}$	$\beta_e^{l_t}$
Mode 1	0.3	0.08	0.1667	0.0083	0.2	2	0.42	1	1	0.2
Mode 2	0.263	0.083	0.125	0.01875	0.31	2.4	0.35	0.5	1	0.31
Mode 3	0.244	0.083	0.125	0.0083	0.15	1.6	0.33	1	1	0.15

Table 3. Parameter values.

Value of γ	Value of π	Value of Ω	Value of K
$\gamma_1 = 100$	$\pi_{mn1} = \begin{bmatrix} -0.3 & 0.15 & 0.15 \\ 0.2 & -0.6 & 0.4 \\ 0.15 & 0.15 & -0.3 \end{bmatrix}$	$\Omega_1 = 10^5 \times \begin{bmatrix} 1.3749 & 0.0013 \\ 0.0013 & 0.2930 \end{bmatrix}$	$K_{11} = [-0.3776 \ -0.01335]$ $K_{12} = [-0.3340 \ -0.0132]$ $K_{13} = [-0.8766 \ -0.0306]$
$\gamma_2 = 10$	$\pi_{mn2} = \begin{bmatrix} -0.37 & 0.186 & 0.186 \\ 0.231 & -0.673 & 0.442 \\ 0.151 & 0.151 & -0.302 \end{bmatrix}$	$\Omega_2 = 10^3 \times \begin{bmatrix} 1.3749 & 0.0013 \\ 0.0013 & 0.2930 \end{bmatrix}$	$K_{21} = [-0.3621 \ -0.0110]$ $K_{22} = [-0.3221 \ -0.0102]$ $K_{23} = [-0.8523 \ -0.0242]$
$\gamma_3 = 1$	$\pi_{mn3} = \begin{bmatrix} -0.37 & 0.185 & 0.185 \\ 0.231 & -0.673 & 0.442; \\ 0.151 & 0.151 & -0.302 \end{bmatrix}$	$\Omega_3 = \begin{bmatrix} 1.3319 & 0.0012 \\ 0.0012 & 0.2830 \end{bmatrix}$	$K_{31} = [-0.3924 \quad 0.0012]$ $K_{32} = [-0.5045 \quad 0.0014]$ $K_{33} = [-1.1241 \quad 0.0220]$

Based on all the provided parameters, we conducted simulation analysis using MATLAB and obtained the system trajectories under different performance indices γ and varying transition probabilities π_{mn}.

First, it can be clearly observed from Figure 2 that when no control signal is applied, the state variables of the power system exhibit relatively severe fluctuations. These fluctuations are not only large in amplitude but also high in frequency, making it difficult for the system to maintain stable operation. This indicates that without effective control strategy intervention, the system struggles to remain within an ideal operating range, potentially leading to issues such as significant frequency deviations and power imbalances, thereby compromising the safety and reliability of the entire power system.

Additionally, compared to Figure 2, the state variables in Figures 3–5 under the action of control signals can not only rapidly reach a stable state but also maintain excellent stability in subsequent phases. Despite the presence of initial disturbances $w(t)$), communication delays $\tau(t)$, and stochastic mode switching driven by the semi-Markov chain l_t, the state variables can effectively converge to a very small neighborhood around the equilibrium point within a finite time. This fully demonstrates the effectiveness of the proposed control strategy in regulating the power system and its significant role in ensuring the system's stochastic stability and achieving H_∞ performance.

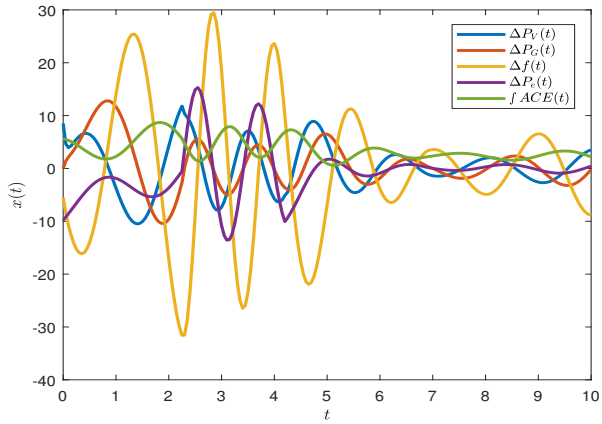

Figure 2. State variable trajectory evolution without control input.

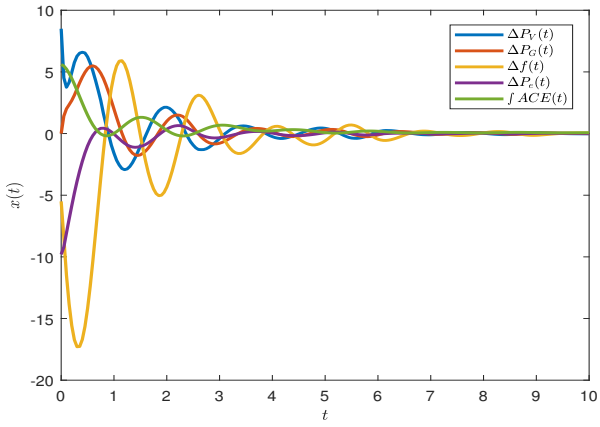

Figure 3. State variable trajectory evolution ($\gamma = 100$).

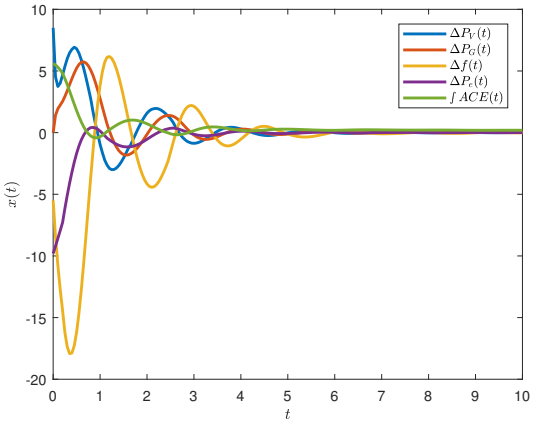

Figure 4. State variable trajectory evolution ($\gamma = 10$).

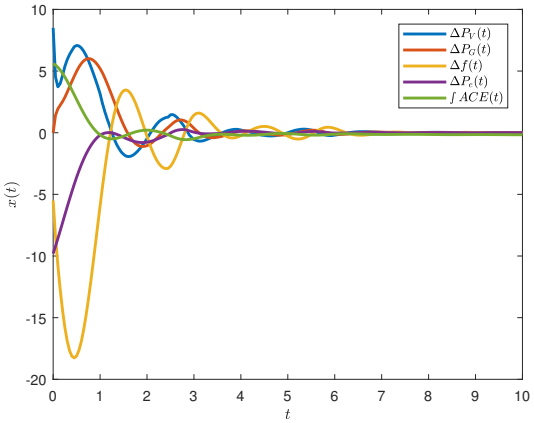

Figure 5. State variable trajectory evolution ($\gamma = 1$).

Notably, according to the simulation results and parameter analysis, as the H_∞ performance index

γ decreases from 100 to 10 and then to 1, the absolute values of the controller gain matrix K generally increase, indicating a gradual enhancement of the controller's regulating effect. Correspondingly, the convergence and robustness of the system's state trajectories significantly improve: when $\gamma_1 = 100$, the state tends to stabilize but still exhibits visible fluctuations; when $\gamma_1 = 10$, the fluctuation amplitude decreases and the convergence speed accelerates; when $\gamma_1 = 1$, the state variables can quickly and smoothly converge to a very small neighborhood near the equilibrium point, demonstrating optimal dynamic performance and anti-disturbance capability. This indicates that a smaller γ value corresponds to stronger control gains and superior system stability.

5.2. Interpretation of the results

In this subsection, we focus on analyzing the evolution of control input signals and the semi-Markov process in power system (2.6) under the condition of $\gamma = \gamma_1$, $\pi = \pi_{mn1}$, $\Omega = \Omega_1$, and $K = K_1$, thereby validating the effectiveness of the proposed AETM.

Figure 6 illustrates the evolution of the control input trajectory. As can be seen from the figure, the control input signal exhibits regular variations during the system operation. These variations are closely related to the dynamic response of the system state variables, indicating that the control strategy can adjust the control input in real-time according to the current state and requirements of the system to achieve precise regulation of the power system. This dynamic adjustment capability not only improves the system's response speed but also enhances its adaptability and robustness, enabling it to maintain good control effects in the face of various uncertainties and disturbances. Figure 7 displays the dynamic characteristics of the continuous semi-Markov process switching between different modes, which reflects the transitions of the power system between different operating states. By introducing the semi-Markov process for modeling, the paper can more accurately capture the temporal characteristics and historical dependence of system mode switching. As can be seen from the figure, the frequency and amplitude of mode switching vary in different time periods, indicating that the system is affected by various factors during operation, such as environmental changes and equipment failures. Through this detailed modeling and analysis, the control strategy proposed in this paper can better adapt to system mode switching, ensuring effective control in different operating states and thereby enhancing the stability and reliability of the entire power system.

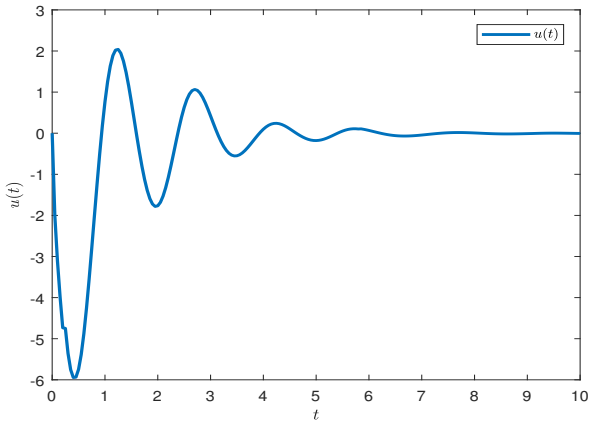

Figure 6. Dynamic variation of the control inputs.

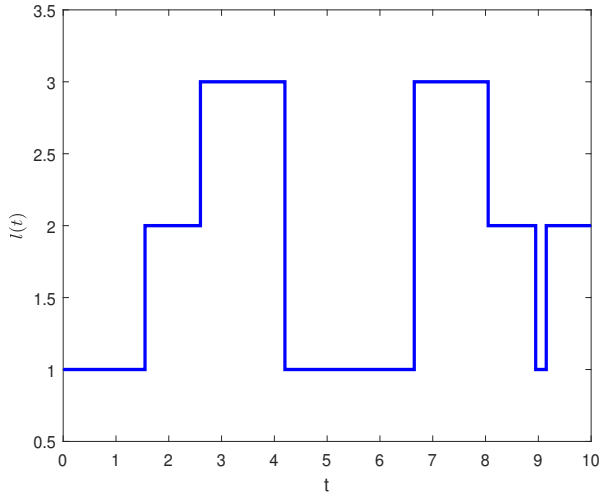

Figure 7. Continuous semi-Markov process.

Figures 8 and 9 respectively illustrate the triggering instances of the conventional ETM and the proposed AETM in this paper. By comparing these two figures, significant differences in triggering time, triggering probability, and maximum triggering interval between the two triggering mechanisms can be clearly observed, as detailed in Table 4. It is worth noting that the number of triggers for the AETM has been significantly reduced from 73 times for the conventional ETM to 30 times, with a triggering rate reduction of 15.7%. In addition, the maximum triggering interval for the AETM has been extended by 0.37 second. The experimental results conclusively validate that the AETM effectively minimizes redundant data transmission in power system implementations, and substantially lessens computational load, thereby optimizing bandwidth utilization and boosting operational performance. This empirical evidence firmly establishes the AETM's capability to dramatically improve both data handling capacity and event-triggering efficiency.

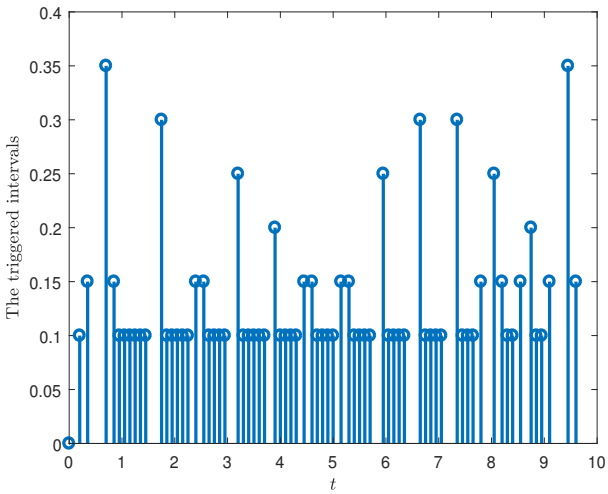

Figure 8. ETM instants.

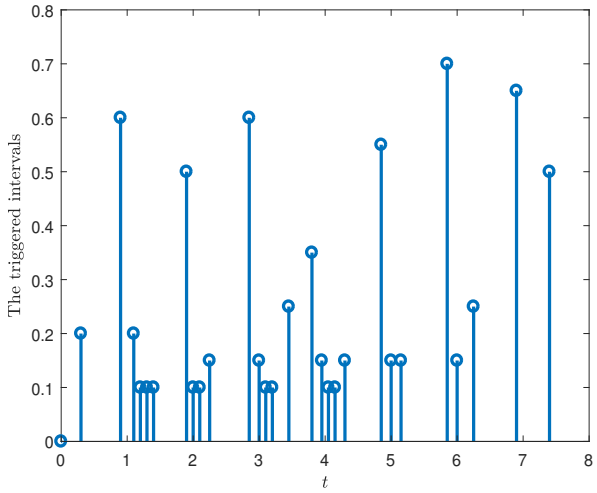

Figure 9. AETM instants.

Table 4. Metrics related to event-triggering strategies.

Type	Total triggers	Proportion of triggers	Maximum trigger interval
ETM	73	36.5%	0.35
AETM	30	15%	0.72
Improvement	43	15.7%	0.37

6. Conclusions

In order to enhance the control efficiency and stability of power systems under complex environmental conditions, this study has investigated the H_∞ LFC of semi-Markov jump power systems with the AETM. Initially, considering the uncertainties in power systems due to environmental factors, a semi-Markov jump process has been utilized for system modeling, effectively capturing the dynamic variations across different operational states. Subsequently, to alleviate the communication and computational burdens, a novel AETM has been proposed, which selectively determines triggering conditions to prevent unnecessary control signal updates. This approach has not only reduced communication costs but also boosted computational efficiency. Building on this foundation, asymmetric multi-modal LKFs that can significantly reduce the conservativeness of stability criteria have been constructed to analyze the system's stability under H_∞ performance. More relaxed criteria imply that the designed controller has a larger stability margin, which not only ensures the system's stability but also enhances its robustness, maintaining the system's robustness even in the presence of external disturbances. Finally, the simulation results have confirmed the effectiveness of this method, which not only significantly improves control performance and stability but also effectively reduces resource consumption. In future work, we will devise a more refined hybrid triggering mechanism that further compresses communication overhead while maintaining system stability; simultaneously, the modeling layer will integrate both semi-Markov jumps and hidden Markov models into the controller framework to enhance the identification of state uncertainties and achieve superior control performance.

Author contributions

Kaibo Shi and Chuan Liu: Constructed the research framework, co-wrote the introduction and conclusion, and oversaw the overall logic and coherence of the manuscript; Yuping Zhang: Handled the collection and processing of experimental data, implemented the data-analysis methodology, and authored the experimental-methods dection, systematically detailing the experimental procedures and the tools employed; Xiangkun Wang: Conducted the literature review, critically analyzing existing studies to provide a solid theoretical foundation, and contributed to the discussion section for an in-depth interpretation of the results; Yanbin Sun: Prepared all figures, ensuring the data are presented clearly and accurately; Xiao Cai: Standardized the manuscript's formatting to comply with publication requirements. All authors have read and approved the final version of the manuscript for publication.

Use of Generative-AI tools declaration

The authors declare that they have used Artificial Intelligence (AI) tools in the creation of this article.

Acknowledgments

This work was supported by the Sichuan Science and Technology Program (Nos. 2025ZNSFSC0460, 25NSFSC2581, and 2024NSFSC2056), China National Postdoctoral Program for Innovative Talents (No. BX20240095), China Postdoctoral Science Foundation (No. 2024M750616), National Natural Science Foundation of China (Nos. 62402129, 62272119, 62372126, 62372129, U2436208, U2468204), Guangdong S&T Program (No. 2024B0101010002), Guangdong Basic and Applied Basic Research Foundation (Nos. 2020A1515010450, 2021A1515012307), and Guangdong Key Laboratory of Industrial Control System Security Project (2024B1212020010).

Conflict of interest

The authors declare no conflicts of interest.

References

1. J. Shair, H. Li, J. Hu, X. Xie, Power system stability issues, classifications and research prospects in the context of high-penetration of renewables and power electronics, *Renew. Sust. Energ. Rev.*, **145** (2021), 111111. https://doi.org/10.1016/j.rser.2021.111111
2. M. O. Qays, I. Ahmad, D. Habibi, A. Aziz, T. Mahmoud, System strength shortfall challenges for renewable energy-based power systems: A review, *Renew. Sust. Energ. Rev.*, **183** (2023), 113447. https://doi.org/10.1016/j.rser.2023.113447
3. N. M. Manousakis, P. S. Karagiannopoulos, G. J. Tsekouras, F. D. Kanellos, Integration of renewable energy and electric vehicles in power systems: A review, *Processes*, **11** (2023), 1544. https://doi.org/10.3390/pr11051544

4. K. D. Lu, Z. G. Wu, Resilient event-triggered load frequency control for cyber-physical power systems under dos attacks, *IEEE Trans. Power Syst.*, **38** (2022), 5302–5313. https://doi.org/10.1109/TPWRS.2022.3229667
5. F. Mohammadi, B. Mohammadi-Ivatloo, G. B. Gharehpetian, M. H. Ali, W. Wei, O. Erdinç, et al., Robust control strategies for microgrids: A review, *IEEE Syst. J.*, **16** (2022), 2401–2412. https://doi.org/10.1109/JSYST.2021.3077213
6. A. M. Eltamaly, A. A. Z. Diab, A. G. Abo-Khalil, Robust control based on H_∞ and linear quadratic gaussian of load frequency control of power systems integrated with wind energy system, In: *Control and operation of grid-connected wind energy systems*, Cham: Springer, 2021, 73–86. https://doi.org/10.1007/978-3-030-64336-2_4
7. T. Sasaki, K. Enomoto, Dynamic analysis of generation control performance standards, *IEEE Trans. Power Syst.*, **17** (2002), 806–811. https://doi.org/10.1109/TPWRS.2002.800946
8. X. Zhao, Z. Ma, S. Li, S. Zou, Robust lfc of power systems with wind power under packet losses and communication delays, *IEEE J. Emerg. Sel. Top. Circuits Syst.*, **12** (2022), 135–148.
9. H. Zhan, J. Wu, L. Cheng, X. Zhan, H. Yan, Design of H_∞ control strategies with dynamic event-triggered scheme under markovian deception attacks, *Int. J. Control Autom. Syst.*, **22** (2024), 3108–3116. https://doi.org/10.1007/s12555-024-0423-1
10. S. Liu, C. Duan, W. Zhou, Event-triggering control of networked control systems under random deception attacks: An adaptive triggering strategy with saturation constraint, *Int. J. Control Autom. Syst.*, **21** (2023), 2916–2926. https://doi.org/10.1007/s12555-022-0502-0
11. G. Zhang, J. Li, O. Bamisile, Y. Xing, D. Cai, Q. Huang, An H_∞ load frequency control scheme for multi-area power system under cyber-attacks and time-varying delays, *IEEE Trans. Power Syst.*, **38** (2022), 1336–1349. https://doi.org/10.1109/TPWRS.2022.3171101
12. M. S. Aslam, X. Dai, H_∞ control for network T-S fuzzy systems under time varying delay for multi-area power systems, *Int. J. Control Autom. Syst.*, **18** (2020), 2774–2787. https://doi.org/10.1007/s12555-019-0844-4
13. S. Zhao, L. Zhao, S. Wen, L. Cheng, Secure synchronization control of markovian jump neural networks under DoS attacks with memory-based adaptive event-triggered mechanism, *Artif. Intell. Sci. Eng.*, **1** (2025), 64–78. https://doi.org/10.23919/AISE.2025.000006
14. S. Dong, M. Liu, Adaptive fuzzy asynchronous control for nonhomogeneous markov jump power systems under hybrid attacks, *IEEE Trans. Fuzzy Syst.*, **31** (2022), 1009–1019. https://doi.org/10.1109/TFUZZ.2022.3193805
15. A. Kazemy, M. Hajatipour, Event-triggered load frequency control of markovian jump interconnected power systems under denial-of-service attacks, *Int. J. Electr. Power Energy Syst.*, **133** (2021), 107250. https://doi.org/10.1016/j.ijepes.2021.107250
16. X. Wang, B. Xu, J. Ding, C. Ren, Q. Zhang, Finite-time H_∞ fault detection for large-scale power system via markov jumping mechanism, *IET Control Theory Appl.*, **18** (2024), 2886–2898. https://doi.org/10.1049/cth2.12732

17. X. Cai, K. Shi, Y. Sun, J. Cao, S. Wen, Z. Tian, Intelligent event-triggered control supervised by mini-batch machine learning and data compression mechanism for T-S fuzzy NCSs under DoS attacks, *IEEE Trans. Fuzzy Syst.*, **32** (2023), 804–815. https://doi.org/10.1109/TFUZZ.2023.3308933

18. D. Ding, Z. Tang, C. Wen, Z. Ji, J. H. Park, Secure impulsive synchronization for derivatively coupled networks against DoS attacks: A memory-compensated strategy, *Syst. Control Lett.*, **193** (2024), 105939. https://doi.org/10.1016/j.sysconle.2024.105939

19. B. Li, L. Zhao, S. Wen, Periodic event-triggered consensus of stochastic multi-agent systems under switching topology, *Artif. Intell. Sci. Eng.*, **1** (2025), 147–156. https://doi.org/10.23919/AISE.2025.000011

20. D. Yue, E. Tian, Q. L. Han, A delay system method for designing event-triggered controllers of networked control systems, *IEEE Trans. Automat. Cntrol*, **58** (2012), 475–481. https://doi.org/10.1109/TAC.2012.2206694

21. Y. Chen, C. Wan, P. Cheng, Event-triggered stochastic model predictive control based on distributionally robust optimization approach for network control systems under DoS attacks, *Signal Process.*, **238** (2026), 110–182. https://doi.org/10.1016/j.sigpro.2025.110182

22. S. Dharani, R. Rakkiyappan, J. Cao, Robust stochastic sampled-data H_∞ control for a class of mechanical systems with uncertainties, *J. Dyn. Sys., Meas. Control*, **137** (2015), 101008. https://doi.org/10.1115/1.4030800

23. J. Yang, Q. Zhong, K. Shi, S. Zhong, Dynamic-memory event-triggered H_∞ load frequency control for reconstructed switched model of power systems under hybrid attacks, *IEEE Trans. Cybernet.*, **53** (2023), 3913–3925. https://doi.org/10.1109/TCYB.2022.3170560

24. M. Shen, X. Wang, S. Zhu, Z. Wu, T. Huang, Data-driven event-triggered adaptive dynamic programming control for nonlinear systems with input saturation, *IEEE Trans. Cybernet.*, **54** (2024), 1178–1188. https://doi.org/10.1109/TCYB.2023.3337779

25. D. Ding, Z. Tang, J. H. Park, Z. Ji, Quasi-bipartite synchronization of derivatively coupled complex dynamic networks: Memory-based self-triggered approach, *IEEE Trans. Syst. Man Cybern. Syst.*, **54** (2024), 1611–1621. https://doi.org/10.1109/TSMC.2023.3328426

26. X. C. Shangguan, C. K. Zhang, Y. He, L. Jin, L. Jiang, J. W. Spencer, et al., Robust load frequency control for power system considering transmission delay and sampling period, *IEEE Trans. Ind. Inform.*, **17** (2021), 5292–5303. https://doi.org/10.1109/TII.2020.3026336

27. C. K. Zhang, Y. He, L. Jiang, M. Wu, Notes on stability of time-delay systems: Bounding inequalities and augmented lyapunov-krasovskii functionals, *IEEE Trans. Automat. Cntrol*, **62** (2016), 5331–5336. https://doi.org/10.1109/TAC.2016.2635381

28. Z. Lian, Y. He, C. K. Zhang, M. Wu, Further robust stability analysis for uncertain takagi–sugeno fuzzy systems with time-varying delay via relaxed integral inequality, *Inf. Sci.*, **409** (2017), 139–150. https://doi.org/10.1016/j.ins.2017.05.017

29. R. Abolpour, M. Dehghani, H. A. Talebi, Stability analysis of systems with time-varying delays using overlapped switching lyapunov krasovskii functional, *J. Franklin Inst.*, **357** (2020), 10844–10860. https://doi.org/10.1016/j.jfranklin.2020.08.018

30. M. Rouamel, S. Gherbi, F. Bourahala, Robust stability and stabilization of networked control systems with stochastic time-varying network-induced delays, *Trans. Inst. Meas. Control*, **42** (2020), 1782–1796.

31. S. Wen, X. Yu, Z. Zeng, J. Wang, Event-triggering load frequency control for multiarea power systems with communication delays, *IEEE Trans. Ind. Electron.*, **63** (2016), 1308–1317. https://doi.org/10.1109/TIE.2015.2399394

32. A. Seuret, F. Gouaisbaut, Wirtinger-based integral inequality: Application to time-delay systems, *Automatica*, **49** (2013), 2860–2866. https://doi.org/10.1016/j.automatica.2013.05.030

33. P. Park, J. W. Ko, C. Jeong, Reciprocally convex approach to stability of systems with time-varying delays, *Automatica*, **47** (2011), 235–238. https://doi.org/10.1016/j.automatica.2010.10.014

34. Q. L. Han, Y. Liu, F. Yang, Optimal communication network-based H_∞ quantized control with packet dropouts for a class of discrete-time neural networks with distributed time delay, *IEEE Trans. Neural Netw. Learn. Syst.*, **27** (2016), 426–434. https://doi.org/10.1109/TNNLS.2015.2411290

35. A. Kazemy, J. Lam, X. M. Zhang, Event-triggered output feedback synchronization of master–slave neural networks under deception attacks, *IEEE Trans. Neural Netw. Learn. Syst.*, **33** (2022), 952–961. https://doi.org/10.1109/TNNLS.2020.3030638

36. L. Hu, P. Shi, B. Huang, H_∞ control for sampled-data linear systems with two markov processes, *Optim. Control Appl. Meth.*, **26** (2005), 291–306. https://doi.org/10.1002/oca.761

AIMS Press